TRANSIENT MODAL ANALYSIS OF NONLINEAR ROTOR-BEARING SYSTEMS

Richard W. Armentrout and **Edgar J. Gunter**

RODYN Vibration Analysis, Inc.
1932 Arlington Boulevard
Charlottesville, VA 22903-1560

ABSTRACT

Recent advances in digital computing resources have made the analysis of large nonlinear rotor-bearing systems practical in a desktop computing environment. With modern personal computers and workstations, it is now possible to perform large time transient numerical solutions of nonlinear models that previously could only be approximated as linear systems due to limitations in computing capabilities. Summarized in this paper is a transient rotordynamic analysis based on modal techniques that incorporates an efficient model for a nonlinear squeeze film damper. An application is presented in which the analysis is used to predict nonlinear unbalance response in an aircraft turbofan engine for the optimization of squeeze film damper and bearing support characteristics. The efficiencies of the modal approach yield typical run times of less than 20 minutes on a 300 MHz desktop computer.

NOMENCLATURE

[M]	mass matrix
[K]	stiffness matrix
[C]	damping matrix
[I]	diagonal identity matrix
[ϕ]	mode shape matrix
{q}	modal displacement vector
{u}	physical displacement vector
F	physical force
P	pressure
R	damper radius
L	damper length
X,Y,Z	translational coordinates
c	damper set clearance
f	modal force
h	film thickness
t	time
ϕ	phase angle
$\theta_x\theta_y,\theta_z$	angular coordinates
μ	viscosity

INTRODUCTION

Vibration analysis of rotor-bearing systems has historically contained a number of approximations due to the limitations in computing resources and, in some cases, an incomplete understanding of the physics involved. One common approximation that remains prevalent even today is the assumption of linearity. By approximating a nonlinear structural system as linear, the model may be constructed of ordinary differential equations that are easily solved in closed form, thereby minimizing the computing requirements. In a steady-state linear solution of rotor unbalance response, the rotor, bearing, and any support structure such as bearing pedestals are modeled using well known beam theory for the rotor and lumped parameter or plate/shell theory for the foundation. A global system of mass, stiffness, and damping matrices is constructed with the nonlinear elements assumed to behave linearly about an equilibrium position. With these "linearized" oil film and seal coefficients inserted properly into the system matrices, a harmonic solution is assumed of the form

$$X(t) = \bar{X}e^{i\omega t} = X_r\cos(\omega t) + X_i i\sin(\omega t) \qquad (1)$$

with a forcing function of the form

$$F(t) = \bar{F}e^{i\omega t} = F_r\cos(\omega t) + F_i i\sin(\omega t) \qquad (2)$$

Using complex variables, the solution of forced rotor response to unbalance is easily achieved in closed form for each rotor speed. While economical and straightforward computationally, this approach neglects important aspects of the physics acting in many systems which contain nonlinear elements or become subjected to transient events. One such system is a rotor running in oil film bearings or squeeze film dampers. In such a system, the assumption of linearity can overlook important effects such as asynchronous whirl, limit cycles, nonlinear jumps, and dry rubs.

A more general and comprehensive approach for computing forced vibration in rotor systems is through time transient

numerical integration. A number of researchers [1-6] have developed and applied transient methods in rotordynamics. With a transient analysis, the rotor model degrees of freedom are marched forward in time through a force balance at each time step. This allows any nonlinear elements to be included directly as long as their forces can be represented as a function of position and velocity states. Supersynchronous and subsynchronous vibrations are included implicitly in transient analyses because of the absence of the synchronous harmonic restriction. Transient events are also characterized inherently by a transient marching solution as long the time steps are fine enough to simulate the transient disturbance and the resulting response. It is because of this generality that transient solutions are such powerful tools for simulating the wide variety of effects that can play in rotordynamics simulations.

ROTOR-SUPPORT MODEL

Illustrated in Figure 1 is a general two-level rotor-support model showing the major components represented by the transient analysis model. The first level outboard of the shaft is labeled the "oil film" and connects the rotor with the pedestal supports. The oil film may be one of a number of different linear or nonlinear elements including fixed-geometry bearings, tilting pad bearings, labyrinth seals, or squeeze film dampers. These are represented by direct and cross-coupled stiffness and damping coefficients in a linear model, or by state-dependent forces in a nonlinear analysis. In the current transient analysis, the oil film consists of a squeeze film damper model based on a closed form pressure integration.

Outboard of the oil film is a lumped-mass support model that can represent support structures such as bearing pedestals, turbocharger housings, or simple engine casings. The outer-most level connecting the pedestals to ground is represented by constant damping coefficients and stiffness coefficients having either linear, quadratic, or cubic force-displacement characteristics. The stiffness and damping coefficients in the support model contain both principle and cross-coupled terms.

MODAL REPRESENTATION

In a modal transient solution, the undamped or damped modes are first computed and the resulting eigenvalues and eigenvectors are used to transform the physical equations into a reduced set of modal equations. A transformation of coordinates is then implemented as follows, based on the system vibration characteristics

$$\{u\}_n = [\phi]_{nxm}\{q\}_m \tag{3}$$

where {u} is the vector containing the physical nodal displacements of the system, [ϕ] is the matrix whose columns are the eigenvectors, and {q} is the vector containing the modal displacements. The subscripts n and m are the number of physical degrees of freedom and the number of modes retained, respectively. The modal equations represent the complete physical system with an uncoupled set of modal coordinates, rather than a coupled set of physical coordinates. This approach is appealing in that it allows the deletion of

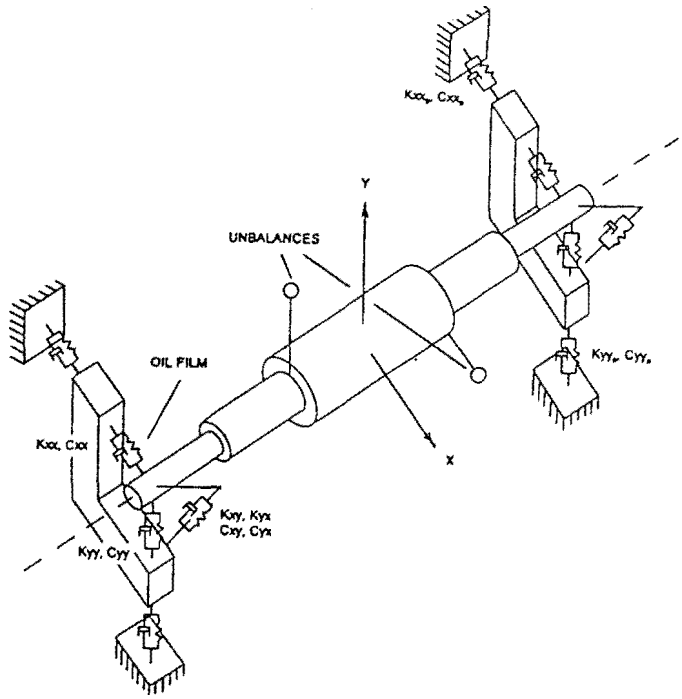

Figure 1. Two-Level Rotor Model.

higher frequency modes that have little participation in the dynamic response, yielding significantly fewer degrees of freedom than the original physical model. Similar methods have been used for transient simulations by Adams [3], Choy [4], and Hassenpflug [5].

MODAL EQUATIONS OF MOTION

Development of the modal equations of motion begins with the general second order differential equation of motion expressed in matrix form as

$$[M]\{\ddot{u}(t)\} + [C]\{\dot{u}(t)\} + [K]\{u(t)\} = \{F(t)\} \tag{4}$$

For computation of the real modes, the damping and forcing function are dropped, leaving the undamped homogeneous equation

$$[M]\{\ddot{u}(t)\} + [K]\{u(t)\} = 0 \tag{5}$$

Assuming a solution of the form

$$u(t) = Ae^{i\omega t} \tag{6}$$

then the second derivative becomes

$$\ddot{u}(t) = -\omega^2 u(t) \tag{7}$$

Substituting Equation 7 into the homogenous equation of motion yields the standard undamped eigenvalue equation

$$\left[[M]^{-1}[K] - \omega_i^2[I]\right]\{Y_i\} = 0 \tag{8}$$

Where γ_i are the eigenvectors, from which the orthonormal modes may be computed as

$$\{\phi_i\} = \frac{\{\gamma_i\}}{\sqrt{\{\gamma_i\}^T[M]\{\gamma_i\}}} \quad (9)$$

The orthogonality conditions for the modes are

$$\{\phi_i\}^T[M]\{\phi_i\} = [I] \quad \textit{and} \quad \{\phi_i\}^T[K]\{\phi_i\} = [\omega_i^2] \quad (10)$$

Returning to the undamped rotor equation of motion given in Equation 5, we now add the unbalance forces, support forces, and gyroscopic forces on the right side and drop the time dependence to give the non-homogeneous equation of motion as

$$[M]\{\ddot{u}\} + [K]\{u\} = \{F_{ub}\} + \{F_{sup}\} + \{F_{gyr}\} = \{F_t\} \quad (11)$$

where

F_t = ***Total Force Vector.***
F_{ub} = ***Unbalance Forces.***
F_{sup} = ***Support Forces.***
F_{gyr} = ***Gyroscopic Forces.***

The unbalance forces for any station, i, are defined by the unbalance masses, M_{ub}, eccentricity, e, and phase angle, ϕ, for station i as

$$\begin{Bmatrix} Fx_{ub} \\ Fy_{ub} \end{Bmatrix}_i = \begin{Bmatrix} M_{ub}\, e\, \omega^2 \cos(\omega t + \phi) \\ M_{ub}\, e\, \omega^2 \sin(\omega t + \phi) \end{Bmatrix}_i \quad (12)$$

The gyroscopic moments for small displacements without rotor acceleration effects are

$$\begin{Bmatrix} Mx_{gyr} \\ My_{gyr} \end{Bmatrix}_i = \begin{Bmatrix} -\omega I_p \dot{\theta}_y \\ \omega I_p \dot{\theta}_x \end{Bmatrix}_i \quad (13)$$

Note that the gyroscopics forces couple the rotor horizontal and vertical responses, but the modes can remain in uncoupled form as long as the forces are applied on the right side of Equation 11.

The modal transformation is based on the assumption that the physical responses are expressible as a linear combination of the modal responses transformed by the mode shapes as

$$\{u\} = [\phi]\{q\} \quad (14)$$

Substituting this transformation into Equation 11 yields

$$[M][\phi]\{\ddot{q}\} + [K][\phi]\{q\} = \{F_t\} \quad (15)$$

Premultiplying both sides by the transpose of the mode shapes gives

$$[\phi]^T[M][\phi]\{\ddot{q}\} + [\phi]^T[K][\phi]\{q\} = [\phi]^T\{F_t\} \quad (16)$$

Substituting in the orthogonality relations of Equation 10 yields the uncoupled modal equations of motion as

$$\{\ddot{q}\} + [\omega^2]\{q\} = \{f\} \quad (17)$$

where $\{f\}$ is now the modal force vector after transformation to modal space. Since the modes remain uncoupled, the modal equations may be solved individually as

$$\ddot{q}_i + \omega_i^2 q_i = f_i \quad (18)$$

It is common to include the effects of material damping in the rotor through a modal damping term, ζ_i, for each mode to yield

$$\ddot{q}_i + 2\omega_i \zeta_i \dot{q}_i + \omega_i^2 q_i = f_i \quad (19)$$

This is the form of the modal equations which are assembled for solution by transient numerical integration with the modal forces, f_i, and the modal responses, q_i, evaluated at each time step. An iterative predictor-corrector integration scheme is implemented using a central difference predictor step in combination with a Newmark Beta corrector step.

SQUEEZE FILM DAMPER MODEL

Current trends in turbomachinery design for increased operating speeds and higher specific power levels have led to lighter and more flexible rotor-bearing systems. With the higher power levels also come increased fluid pressure gradients that introduce more of the destabilizing forces associated with fluid cross-coupling effects. Consequently, there are an increasing number of designs that require the supplemental damping of a squeeze film damper mounted concentrically with the existing oil film or rolling element bearings to help attenuate the vibration response. This is especially true in applications such as aircraft engines that use rolling element bearings instead of fluid film bearings, where the inherently low damping of the rolling element bearings alone would not be sufficient to attenuate the vibration response as critical speeds are traversed. In such systems, it would often be impossible to run at all without the supplemental damping offered by squeeze film dampers.

Illustrated in Figure 2 are end and cross sectional views of a squeeze film damper showing the geometry and coordinate conventions. The damper consists of inner and outer sleeves separated by a thin film of oil. Often there is a circumferential oil supply groove to distribute oil around the damper. Sometimes there are end seals to allow pressurization of the damper oil film for reduction of cavitation. Other dampers are open on the ends so that the oil drains to the surrounding ambient pressure. Geometrically, a squeeze film damper is very similar to a plain journal bearing except that there is no rotational velocity. Because of this relatively simple geometry that is continuous in the circumferential direction, a squeeze

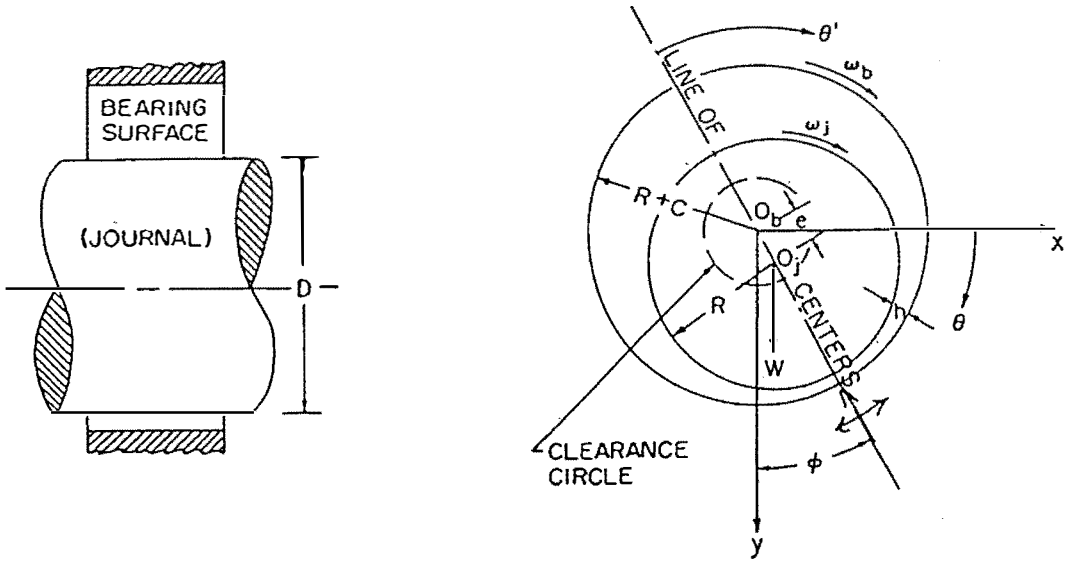

Figure 2. Squeeze Film Damper Geometry.

film damper may be modeled with good accuracy in closed form.

A brief discussion of the theoretical damper pressure and force expressions is given below for understanding of their use in the transient integration model. A full development of the isoviscous squeeze film damper theory is given in [7].

Development of the damper force expressions begins with a second order partial differential fluid equation called Reynolds Equation which is given as

$$\frac{\partial}{\partial z}\left[\frac{h^3}{6\mu}\frac{\partial P}{\partial z}\right] = \omega_j\frac{\partial h}{\partial \theta} + 2\frac{\partial h}{\partial t} \tag{20}$$

If the bearing is relatively short relative to the diameter ($L \le 0.5D$), the parabolic pressure distribution of Figure 3 may be assumed in the axial direction with the peak pressure located at the axial centerline. With this pressure distribution, the pressure gradient, $\partial P/\partial Z$, is zero at $Z=L/2$. The pressure must also drop to xero at Z=0 and Z=L. With these assumptions, the Reynolds Equation may be integrated twice with respect to Z to yield the pressure as

$$P(\theta,Z) = \frac{3\mu}{h^3}(Z^2 - LZ)\left(\omega_j\frac{\partial h}{\partial \theta} + 2\frac{\partial h}{\partial t}\right) \tag{21}$$

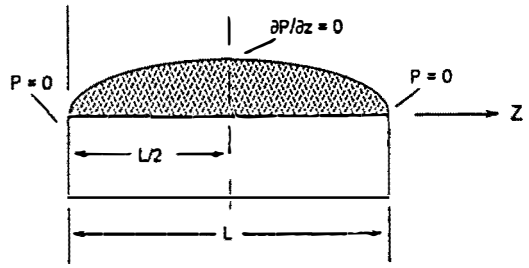

Figure 3. Short Bearing Axial Pressure Profile.

The derivatives of film thickness with respect to θ and t are

$$\frac{\partial h}{\partial \theta} = x\sin(\theta) - y\cos(\theta)$$
$$\frac{\partial h}{\partial t} = -\dot{x}\cos(\theta) - \dot{y}\sin(\theta) \tag{22}$$

The incremental force acting on the journal is expressed in terms of incremental values of θ and z as

$$\Delta F = -P(\theta,Z)R\,d\theta\,dZ \tag{23}$$

The total force components in the x and y directions are found by integrating the incremental forces over the entire journal surface to give

$$F_x = -\int_0^{2\pi}\int_0^L P(\theta,Z)R\cos(\theta)\,dZ\,d\theta$$
$$F_Y = -\int_0^{2\pi}\int_0^L P(\theta,Z)R\sin(\theta)\,dZ\,d\theta \tag{24}$$

Substituting the expressions for $\partial h/\partial\theta$ and $\partial h/\partial t$ into the pressure equation, dropping the journal spin rate, and integrating around the bearing circumference gives the final X and Y direction journal forces as

$$\begin{Bmatrix}F_x\\F_y\end{Bmatrix} = \mu RL^3\int_0^{2\pi}\frac{(\dot{x}\cos(\theta)+\dot{y}\sin(\theta))}{(c - x\cos(\theta) - y\sin(\theta))^3}\begin{Bmatrix}\cos(\theta)\\\sin(\theta)\end{Bmatrix}d\theta \tag{25}$$

This journal force expression was incorporated into the transient analysis for exaluation of the instantaneous damper forces at each integration time step.

AIRCRAFT TURBOFAN ENGINE

An aircraft turbofan engine high pressure (HP) rotor was analyzed using the nonlinear model to predict the sensitivity to varous levels of rotor unbalance. Two in-flight failures involving severe rotor-to-stator rubs were believed to be the result of high unbalance sensitivity caused by the nonlinearities in the original short damper design. Consequently, the objective of the rotordynamic analysis was to establish a set of design recommendations that would help prevent future rub incidents through improvements to the bearing damper design.

Illustrated in Figure 4 is a cross-sectional view of the HP rotor from a finite element model developed to study the rotor centrifugal growth. The running speed range is from idle at 15,000 rpm, to full-throttle at 30,000 rpm. Bearing number 1 at the compressor end is a ball bearing supported in a squeeze film damper, while bearing number 2 is a roller bearing mounted directly to the casing.

Illustrated in Figure 5 is the rotordynamic model developed to compute critical speeds and response of the HP rotor. Mass and inertia properties are lumped at four stations corresponding to the three compressor stages and the turbine stage. The casing substructure was modeled through elastically-supported lumped masses. Substructure stiffnesses of 4.0×10^5 lb/in and 1.5×10^5 lb/in were used the number 1 and number 2 bearing locations, respectively.

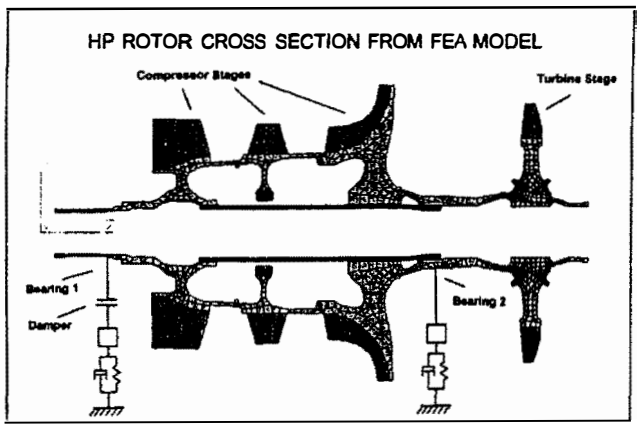

Figure 4. Cross-Sectional View of Engine HP Rotor.

The first three undamped rotor mode shapes and natural frequencies are shown in Figure 6 for the HP rotor with the damper stiffness set to 2.0×10^5 lbf/in. The undamped frequencies do not match exactly the corresponding damped critical speeds because they have constant dynamic coefficients and are without a frequency-dependent force excitation. However, they do characterize very well the general behavior and mode shape of each mode.

The first undamped critical speed at 8891 rpm is the classic first rigid rotor conical mode typical of relatively short, stiff rotors. Because nearly all of the modal compliance is in the number 2 bearing, rather than the rotor, the bearing and support stiffness is the primary modal compliance controlling this mode. With no damper at the number 2 bearing, this mode is poorly damped and exhibits a high amplification factor as it is traversed. Fortunately, at 8891 rpm this mode is well below the running speed range of 15,000 to 30,000 rpm, making it inconsequential as long as the balance condition is good enough to allow safe traversing of this mode during startup and coastdown.

The second critical speed at 19,514 rpm is also a conical mode, however now exhibiting more rotor bending than the first mode. Like the first mode, the primary controlling compliance is from the bearing and substructure, making the modal frequency and response amplitude very sensitive to bearing stiffness and damping changes, respectively. While the computed frequency is 19,514 rpm, it should be remembered that this mode can vary in frequency from approximately 14,000 rpm to 26,000 rpm, depending on the damper effective stiffness and the unbalance. Since the damper stiffness is highly dependent on the whirl amplitude, which in turn is dependent on unbalance, this mode exhibits unbalance-dependent frequency characteristics. Consequently, this mode can be driven well into the operating speed range with the introduction of a large unbalance source or sudden disturbance such as compressor surge.

The third mode is fundamentally different from the first two modes because this is the first flexible-rotor mode, where the bearing and support properties have a minimal effect on the

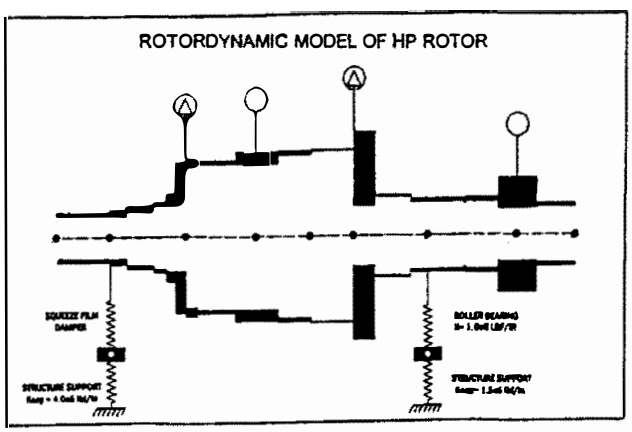

Figure 5. Rotordynamic Model of Engine HP Rotor.

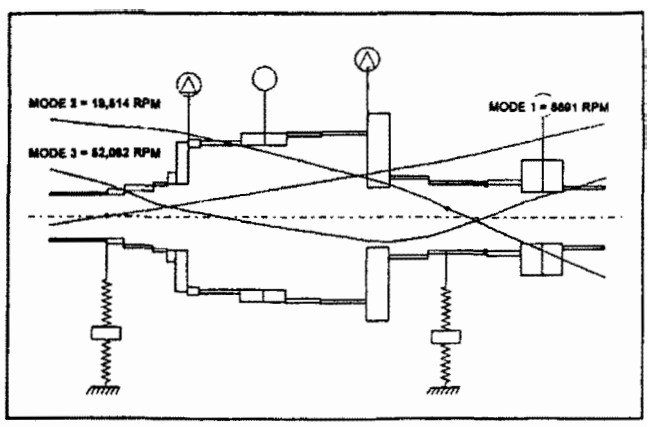

Figure 6. First Three Rotor Undamped Mode Shapes.

frequency or response amplitude and the rotor stiffness is the controlling compliance in the mode. Fortunately, this mode has a much higher computed frequency of 52,082 rpm, placing it well above the rotor operating speed range and making its effects on the rotordynamics inconsequential.

Computed rotor unbalance response at the rub area between compressor stages 2 and 3 is shown for four unbalance levels in Figure 7 with a damper geometry similar to the original "short" damper. The curves were generated by ramping the rotor speed from 5000 rpm to 35,000 rpm over a 30 second time interval. Inspection of the four curves reveals a stationary, linear first mode at approximately 8500 rpm. In contrast, the second mode reflects a dramatic nonlinear effect with an increase in both amplitude and frequency over the unbalance range plotted. The frequency increases from about 14,000 rpm to around 26,000 rpm, while the amplitude varies between 1.5 and 15.0 mils. The increase in frequency can place the second mode well within the operating range of 15,000 rpm to 30,000 rpm if high unbalance develops. At the two highest unbalance levels, there is a nonlinear jump, where the response reaches a point of multiple solutions and suddenly drops to a lower amplitude.

To assess the effects of various damper designs, the unbalance response versus running speed was computed for various damper geometries. Two 0.3 oz-in unbalances were applied, one at the first compressor stage at 0.0 degrees, and one at the turbine stage at 180.0 degrees. This corresponds to a severe 15X unbalance condition that is approximately 15 times the manufacturer's nominal (1X) unbalance condition. The response analysis was conducted using eight free-free rotor modes, two rigid body modes and two flexible body modes in each plane. A time step of 0.00003 seconds was used.

Plotted in Figure 8 are the resulting unbalance responses versus rotor speed at three rotor locations for the original 0.95 inch long damper. Inspection of the curves reveals the first mode resonance at about 8500.0 rpm, and the highly-sensitive second mode resonance near 25,000 rpm with a corresponding nonlinear jump. Under such conditions, the damper effective stiffness is high and the effective damping is low, making the damper less effective and forcing the second critical speed well into the cruise operating speed range of 15,000 rpm to 30,000 rpm. The high stiffness and low damping also cause the second mode to have a relatively high amplification factor that gives a peak bearing 1 response of approximately 0.010 inches (10 mils) at 25,000 rpm.

Similar curves are shown in Figure 9 for an extended-length (1.29 inch) damper with the clearance increasd to 0.007 inches. The curves now indicate better attenuation of the second mode response compared to the original damper, yielding approximately a 25 percent reduction in predicted peak bearing 1 response from 0.010 inches to 0.0075 inches. Opening up the clearance has also yielded a beneficial drop in the predicted second mode frequency from 25,000 rpm to about 21,500 rpm that moves it toward the lower end of the operating speed range.

Under severe conditions, such as compressor surge, it is believed that the rotor experiences a combination of random (broad band) radial impulses as well as an increase in aerodynamic cross-coupling. To simulate the surge event analytically, the rotor was held at a constant 30,000 rpm with

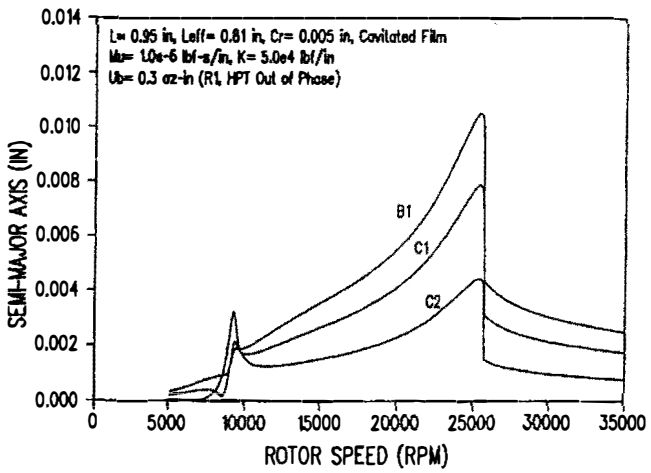

Figure 8. Unbalance Response of HP Rotor With Original Damper at 15X Unbalance.

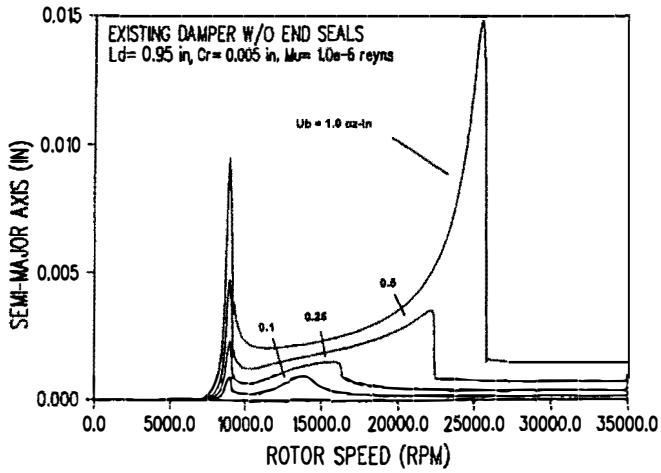

Figure 7. Rub Area Response of HP Rotor Under Increasing Unbalance.

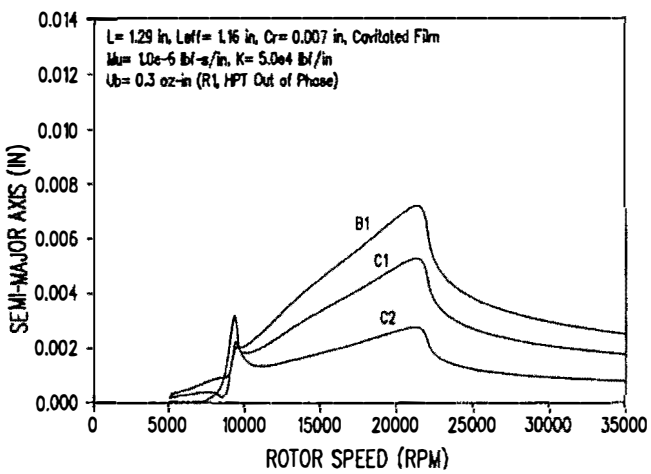

Figure 9. Unbalance Response of HP Rotor With Extended-Length Damper at 15X Unbalance.

an impulse applied to the turbine station at a magnitude of 500.0 lb for 0.001 seconds. Along with the impulse was a suddenly-applied cross-coupling of 8,000 lb/in that was continued throughout the simulation.

The resulting transient response is plotted in Figure 10 for the original damper geometry and support stiffness of 150,000 lb/in. The first several cycles at low amplitude are from a small residual unbalance of 0.05 oz-in and have a frequency of 30,000 cpm corresponding to synchronous unbalance response. After the impulse at 0.5 seconds, the amplitude jumps dramatically as expected. The frequency also drops to about 9300 cpm, which corresponds to the rotor first mode.

To observe the effects of higher bearing 2 support stiffness on the transient response, the transient impulse run was repeated with the support stiffness increased to 300,000.0 lb/in. The extended-length damper with the increased clearance was used. Illustrated in Figure 11 is the resulting transient response, showing a dramatic improvement in sub-synchronous whirl attenuation. The response now exhibits a much better logarithmic decrement of approximately 0.1, and drops very rapidly back to the steady-state value after only 0.15 seconds. This confirms the advantages of the modified damper in combination with a stiffened bearing 2 support for helping attenuate the subsynchronous first-mode whirl.

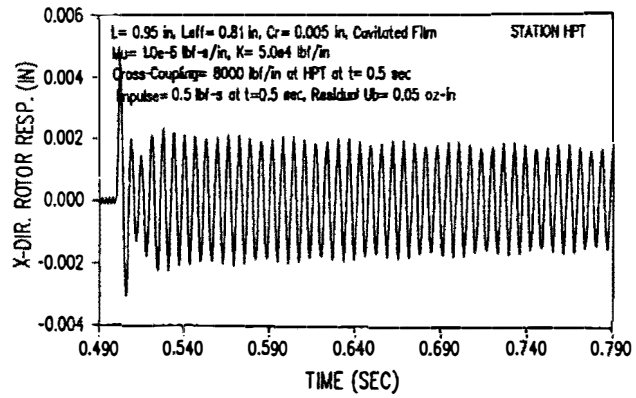

Figure 10. Transient Surge Response of HP Rotor. (Damper L= 0.95 in, C_r= 0.005 in)

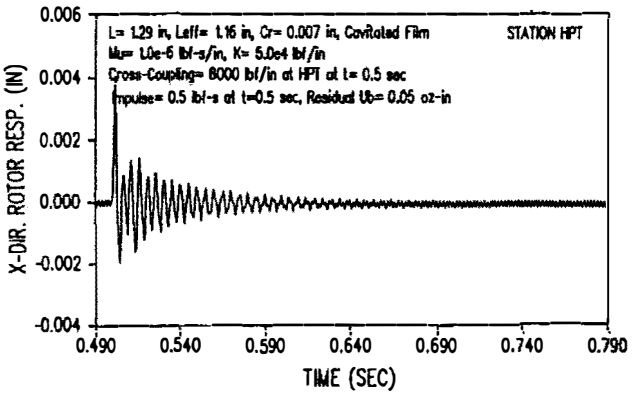

Figure 11. Transient Surge Response of HP Rotor with Increased Brg. 2 Support Stiffness. (Damper L= 1.29 in, C_r= 0.007 in)

CONCLUSIONS

An analytical model has been successfully developed and applied to predict the transient and steady-state behavior of a flexible rotor on nonlinear fluid film supports. A modal approach was used for the rotor that incorporates uncoupled (planar) modes which are acted upon by physical forces transformed into modal coordinates. An application was presented in which an aircraft turbofan engine high-pressure rotor was analyzed to predict the nonlinear unbalance response of the rotor in a squeeze film damper. The primary conclusions which may be drawin from the discussion presented are as follows:

1. A transient rotordynamic analysis may be executed using an uncoupled set of planar rotor modes acted upon by external forces that are transformed into modal coordinates at each time step.

2. Nonlinear support elements such as a squeeze film damper may be modeled efficiently through closed-form integration of the circumferential pressure profile at each integration time step.

3. Nonlinear effects in hydrodynamic supports can change dramatically the response characteristics of rotors under high unbalance, yielding severe vibration that cannot be predicted with a linear analysis.

REFERENCES

[1] **Kirk, R. G., and Gunter, E. J.**, "Transient Response of Rotor-Bearing Systems," *ASME Journal of Engineering for Industry*, May 1974, pp. 682-693.

[2] **Kirk, R. G., and Gunter, E. J.**, "Stability and Transient Motion of a Plain Journal Mounted in Flexible Damped Supports," *ASME Journal of Engineering for Industry*, May 1976, pp. 576-591.

[3] **Adams, M. L.**, "Non-Linear Dynamics of Flexible Multi-Bearing Rotors," *Journal of Sound and Vibration*, February 1980, pp. 129-144.

[4] **Choy, K.C.**, "Dynamic Analysis of Flexible Rotor-Bearing Systems Using a Modal Approach," PhD Dissertation, University of Virginia, August 1977.

[5] **Hassenpflug, H. L.**, "Transient Analysis of Coupled Rotor-Structure Systems," PhD Dissertation, University of Virginia, June 1988.

[6] **Chen, W. J.**, *DYROBES* User's Manual, Eigen Technologies, Incorporated, September, 1998.

[7] **Gunter, E. J., Barrett, L. E., and Allaire, P. E.**, "Design and Application of Squeeze Film Dampers for Turbomachinery Stabilization," Proceedings of the Fourth Turbomachinery Symposium, Texas A&M University, September 1975, pp. 127-141.